Materials Science and Engineering C 62 (2016) 368–376

Contents lists available at ScienceDirect

Materials Science and Engineering C

journal homepage: www.elsevier.com/locate/msec

Effects of Cu content on electrochemical response in Ti-based metallic glasses under simulated body fluid

C.H. Huang [a,1], J.J. Lai [a,1], J.C. Huang [a,*], C.H. Lin [b], J.S.C. Jang [c]

[a] Department of Materials and Optoelectronic Science, National Sun Yat-Sen University, Kaohsiung, Taiwan, ROC
[b] Department of Mechanical and Electro-Mechanical Engineering, National Sun Yat-Sen University, Kaohsiung, Taiwan, ROC
[c] Institute of Materials Science and Engineering; Department of Mechanical Engineering, National Central University, Chung-Li, Taiwan, ROC

ARTICLE INFO

Article history:
Received 28 November 2015
Received in revised form 20 January 2016
Accepted 27 January 2016
Available online 30 January 2016

Keywords:
Corrosion
Metallic glass
Ti alloy
Pitting

ABSTRACT

Systematic characterization of the corrosion response of the Cu-free $Ti_{45}Zr_{40}Si_{15}$ and Cu-containing $Ti_{40}Zr_{40}Si_{15}$–Cu_5 and $Ti_{45}Zr_{20}$–Cu_{35} metallic glasses (MGs) in the Hank's solution is conducted, in terms of the open circuit potential, potentiodynamic polarization, as well as electrochemical impedance measurements. The Cu role in the Ti-based MGs, tentatively to be applied for bio-implants, is established and modeled. The presence of nobler Cu will impose two opposite effects. The minor positive effect of minor shift of E_{corr} is not a major issue, but the negative effect on local pitting and ion release would cause a major drawback. The ICP-MS indicates that the release of Cu ions increases with increasing Cu content. For more promising anti-pitting ability, the Cu content in Ti-based MGs should be kept as low as possible, better to be none or less than about 5 at.%.

1. Introduction

Generally, ideal biomaterials must provide good biocompatibility, non-toxic release, non-allergic responses and proper mechanical properties for biomedical implants and other clinical applications. The mechanical properties, such as strength, load bearing ability and fatigue endurance, are key factors in affecting the operational life of the implants, and these factors would limit the uses of polymers and ceramics [1,2]. In contrast, metals are more favorable materials for orthopedic load-bearing applications due to the sufficient yield strength and cyclic loading resistance [1–3]. Nowadays, the most widely used metals for bio-implants are Ti and Ti-based alloys [4–7]. Unfortunately, the Young's modulus mismatch between Ti-based alloys (~120–140 GPa) and human bones (~5–20 GPa) limits the implant application [1,8]. Moreover, the lower hardness of pure Ti (~1.5 GPa) compared to other metal alloys tends to result in toxic debris releasing after long-term uses due to the unsatisfactory wear resistance [9–12]. Furthermore, Ti-based alloys often contain bio-unfriendly elements, such as Al and V [13]; Al is a growth inhibitor of bone and could cause unwanted Alzheimer's disease and V causes cytotoxicity [14,15].

In contrast to crystalline materials, amorphous metallic glasses (MGs) possess higher tensile strength, lower Young's modulus, larger elastic elongation of about 2%, larger elastic energy, higher corrosion resistance, and good biocompatibility [8,16–22]. The amorphous MGs can be prepared by quenching rapidly from liquid to solid with high cooling rates, preventing the nucleation and growth of crystalline phase(s). Consequently, there are no structural defects in amorphous alloys, such as dislocations, stacking faults, twins and grain boundaries. Because of the homogeneous structure and the lack of periodic crystalline structure, amorphous MGs exhibit some superior physical and chemical properties. In general, the grain boundaries and many other types of defects in crystal materials are the highly chemical-reactive regions that would be preferentially corroded and oxidized. The presence of defects could lead to the formation of inhomogeneous protective oxide layers. There have been various MGs reported for their promising corrosion resistance in comparison with the crystalline materials. Wang et al. [20] demonstrated that the Fe-based MGs have superior pitting corrosion resistance than 316 L stainless steel in Hank's solution. Morrison et al. [23] conducted studies on the different corrosion behaviors of a $Zr_{52.5}Cu_{17.9}Ni_{14.6}Al_{10.0}Ti_{5.0}$ MG and various metals (316 stainless steel, CoCrMo, and Ti–6Al–4V) in phosphate-buffered saline (PBS). Toxic-element-free Ti-based MG ribbons ($Ti_{75}Zr_{10}Si_{15}$ and $Ti_{60}Nb_{15}Zr_{10}Si_{15}$) with comparable corrosion behavior in SBF were investigated by Calin et al. [8] in Ringer's solution. Moreover, Mg-based and Al-based MGs with superior corrosion resistance behavior have been reviewed [24]. For example, the amorphous Al–Fe–Gd, Al–Co–Ce, Al–Ni–Gd, and Al–Ni-Y alloys with approximately 85 at.% Al have all show good resistance against pit stabilization in 0.6 M NaCl solution. And also, Mg–Cu–Y and Mg–Ni–Nd have higher pitting potentials and corrosion current densities compared to Mg-Ni binary alloys. The above results revealed that the MGs are materials with higher corrosion resistance in the Cl-rich corrosive media.

* Correspondent author.
E-mail address: jacobc@mail.nsysu.edu.tw (J.C. Huang).
[1] C. H. Huang and J. J. Lai contributed equally to this work.

http://dx.doi.org/10.1016/j.msec.2016.01.080
0928-4931/

Some previous studies have shown that the Ti-based amorphous MGs have much higher hardness (~5 GPa) and lower Young's modulus (~80–110 GPa) than the crystalline Ti-based alloys (~1–2 GPa and ~120–140 GPa, respectively) [25,26], result in more promising nature such as better wear resistance and reduced stress shielding effects. Besides, Qin et al. [27] have evaluated the corrosion behavior of Ti-based BMGs in Hank's solution compared to that of commercial purity (cp) Ti, and the results revealed that the passive current density is lower than that of cp Ti, demonstrating the more protective and denser passive film formed on the surface of Ti-based BMGs.

There have been a number of Ti-based amorphous systems fabricated so far, for example, Ti-Cu-Ni [28], Ti–Cu–Ni–Co [29], Ti–Cu–Ni–Zr [30] and Ti–Cu–Ni–Zr–Be [31]. In order to increase the glass-forming ability (GFA), elements with smaller atomic radius (r) needed to be added, thus the common Ti-based metallic alloys contain toxic Ni (r ~ 1.24 Å) or Be (r ~ 1.1 Å) [15,32], which limits their applications for biomedical purposes. The Ti–Zr–Cu–Pd and Ti–Zr–Ta–Si amorphous systems without toxic elements [27,33]. Both exhibited higher strength, lower Young's modulus and higher corrosion resistance than pure Ti and Ti–6Al–4V.

The effect of another element with a small atomic size, Cu (r ~ 1.28 Å), also needs to be carefully examined. Most MGs, whether they are Zr-, Mg- or Ti-based, contain Cu to ensure high GFA. However, there have been studies reporting that Cu would impose a harmful impact to human body, causing cytotoxicity or killing cells [32,34]. Our previous studies and the report from Lin et al. [25] showed that the Zr-based MGs without the reactive and cell-toxic Cu element appeared to exhibit more promising corrosion resistance under Cl-rich corrosive media. Moreover, Lu et al. [35] also showed that Zr–Cu MGs with lower Cu contents have better corrosion resistance in 0.01 mol/L HCl solution. Although Cu has been viewed as a bio-unfriendly element to the human body (but not as serious as Ni or Be), studies of Cu effects on the corrosion behavior of Ti-based MGs under SBF are still rare.

In this study, the electrochemical responses of Ti-based amorphous alloys with different Cu contents ($Ti_{45}Zr_{40}Si_{15}$, $Ti_{40}Zr_{40}Si_{15}$–Cu_5 and $Ti_{45}Zr_{20}$–Cu_{35}) are systematically examined for exploring the Cu effects. For the Cu-free $Ti_{45}Zr_{40}Si_{15}$, another element also with a relative small atomic size, Si (r ~ 1.1 Å) compared to Ti and Zr, is substituted to maintain the sufficient GFA. The electrochemical behaviors of these three Ti-based MGs were studied in simulated body fluid (SBF), Hank's solution, by the potentiodynamic polarization measurement and AC impedance testing for evaluating electrochemical kinetic parameters and the structure of passive layers. Then the compositional difference before and after pitting reactions were determined by scanning electric microscopy (SEM) with energy dispersive spectrometry (EDS) mapping. Additionally, after 7-day immersion in SBF, the compositions of the passive layers were determined by X-ray photoelectron spectroscopy (XPS). Finally, the ion release and biocompatibility of Cu-free and Cu-containing Ti-based MGs after potential state test were also evaluated. This study can provide useful information on the effect of Cu content on corrosion properties, which can help in designing promising Ti-based MGs for long-term uses in Cl-rich corrosive environments.

2. Materials and methods

Three amorphous MG ribbons with nominal compositions of $Ti_{45}Zr_{40}Si_{15}$, $Ti_{40}Zr_{40}Si_{15}$–Cu_5 and $Ti_{45}Zr_{20}$–Cu_{35} (all in at.%) were fabricated by melt spinning, starting with pure element of Ti (99.9 wt.%), Zr (99.9 wt.%), Si (99.99 wt.%) and Cu (99.999 wt.%). When the pure metals were heated to melt completely, the melt was poured onto the surface of copper wheel with a high rotation speed of 15 m/s. The melt was then cooled momentarily to result in a thin ribbon measuring 10 mm in width and about 80 μm in thickness. Thermal analysis was carried out by Perkin-Elmer Diamond differential scanning calorimeter (DSC) under an argon atmosphere at a constant heating rate of 40 K/min. Before the structure and composition confirmations and electrochemical experiments, all specimens were abraded by P4000-grit abrasive papers and cleaned by acetone, ethanol and DI water for 10 min. The amorphous structure was confirmed by Bruker D8 X-ray diffractometry (XRD) with monochromatic Cu-Kα radiation (λ = 1.5406 Å) and operated at 40 kV and 40 mA at room temperature. The scanning rate was 1.5°/min. The JEOL JSM-6330 SEM with EDS was used to verify whether the compositions of the metallic ribbons were mixed homogeneously. Transmission electron microscopy (TEM) was used for determining whether the atomic structure of $Ti_{45}Zr_{40}Si_{15}$ ribbon is amorphous or not, using the FEI E.O Tecnai F20 G2 MAT S-TWIN Field Emission TEM operated at 200 kV. The cross-sectional TEM foil was fabricated by the standard process using the SEIKO SMI 3050 dual focused ion beam (FIB) system.

The electrochemical properties and corrosion behaviors were characterized by various kinds of electrochemical measurements. The SBF, isostatic Hank's solution (with a composition of 0.137 M of NaCl, 5.4 mM of KCl, 0.25 mM of Na_2HPO_4, 0.44 mM of KH_2PO4, 1.3 mM of $CaCl_2$, 1.0 mM of $MgSO_4$, and 4.2 mM of $NaHCO_3$), was used as the corrosive media. The samples immersed in the Hank's solution (pH: 7.3) at 310 K (37 °C) were studied by potentiodynamic polarization measurements and electrochemical impedance spectroscopy conducted by the CHI 614D electrochemical work station in a three-electrode cell. A 24 mm^2 platinum plate (larger than the specimens) was used as counter electrode, and the Ag/AgCl was selected as the reference electrode. The

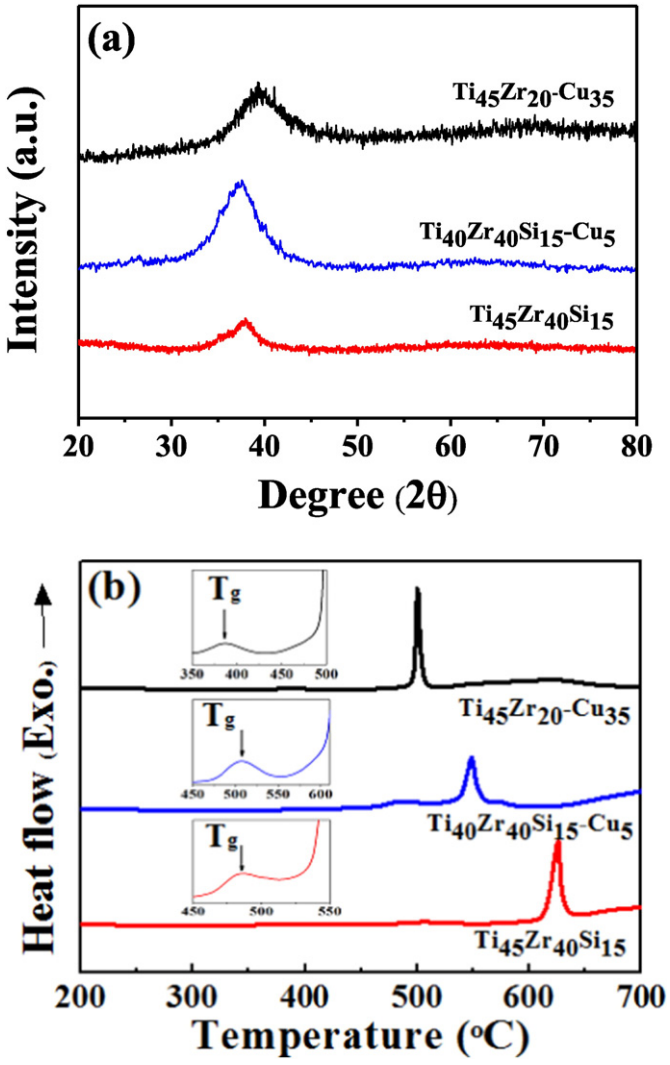

Fig. 1. (a) XRD and (b) DSC patterns of the $Ti_{45}Zr_{40}Si_{15}$, $Ti_{40}Zr_{40}Si_{15}$–Cu_5 and $Ti_{45}Zr_{20}$–Cu_{35} MGs.

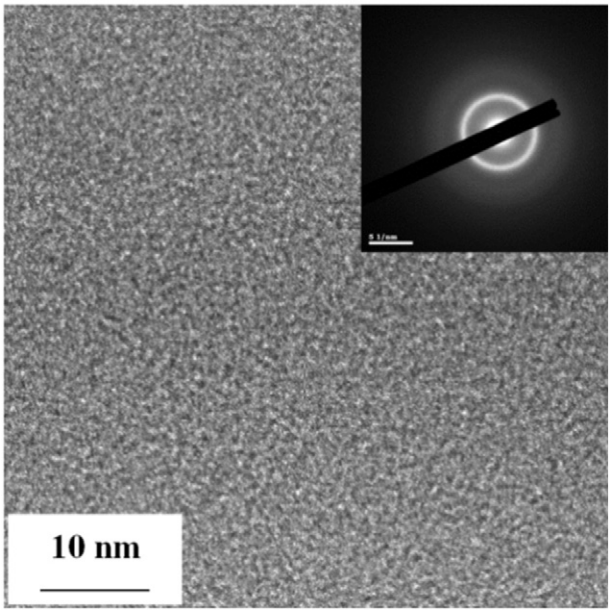

Fig. 2. Bright field TEM image and SAED pattern of the $Ti_{45}Zr_{40}Si_{15}$ ribbon.

samples with 16 mm^2 area (wheel side of the ribbons) immersed in the Hank's solution were used as working electrodes. Before starting the potentiodynamic polarization measurements and AC impedance tests, all of the specimens were immersed in the Hank's solution for 12,500 s until the open circuit potential (OCP) changes were less than 2 mV per 5 min. The impedance test was carried out in the frequency from 10^{-2} to 10^{5} Hz and the amplitude was set to 10 mV around the OCP. The polarization scans started from 0.2 V below the OCP until the occurrence of pitting at a scanning rate of 0.33 mV/s. EDS mapping was used to analyze the compositions of specimens before and after chloride-induced pitting. Each experiment above was repeated for at least 3 times.

All ribbon specimens with 80 μm in thickness were sliced to small pieces with 16 mm^2 exposure area, and then were immersed in Hank's solution under standard atmospheric condition in room temperature (about 25 °C) for 7 days. Before immersing in Hank's solution, the samples were abraded by P4000-grint abrasive and cleaned by acetone, alcohol and D1 water for 10 min. The XPS with Mg–Ka (1253.6 eV) radiation under the vacuum pressure of 10^{-7} Pa operated at 10 kV and 5 mA was conducted to identify the compositions of passive layers formed after long-term immersion. The scan step, dwell time, and passing energy were 0.2 eV, 100 ms, and 50 eV for each narrow scan, respectively. The binding energy peaks of each element were calibrated by the carbon C-1s peak.

In addition, materials were exposed to a membrane potential (about 75–80 mV) to determine ions release and mimic the possible electrochemical reaction between the Cu-free and Cu-containing Ti-based MGs. Potentiostatic polarization measurements with a small applied voltage of 80 mV for 30 min were carried out. Inductively coupled plasma-mass spectrometry (ICP-MS) was utilized to determine the ion concentration in the solution. Even though the membrane potential is not the environmental condition for the implanted Ti-based MG, the implanted MG would suffer from a small potential while activating the surrounding cells due neuron transduction or environmental activations. Therefore, the cell membrane potential would be the highest electrical potential which the implanted metal should sustain. This study evaluated the corrosion risk for the implanted MG under the existence of a possible membrane potential.

3. Results and discussion

3.1. Structural characterization and thermal analysis

Ti-based MGs have better superior mechanical properties than cp Ti for biomedical purposes, due to their special atomic structure, which needs to be confirmed firstly by XRD, as shown in Fig. 1(a). It can be seen that the XRD patterns exhibit a hump instead of discrete sharp Bragg peaks, indicating the dominant amorphous structure. Moreover, the thermal properties were traced by the DSC curves, in which obvious glass transition and crystallization temperatures (T_g and T_x) can be seen, as shown in Fig. 1(b). The T_g and T_x temperatures of $Ti_{45}Zr_{40}Si_{15}$ are 507 and 612 °C, of $Ti_{40}Zr_{40}Si_{15}$–Cu_5 are 485 and 537 °C, and of $Ti_{45}Zr_{20}$–Cu_{35} are 386 and 495 °C, respectively. The presence of T_g and T_x directly supports that the Cu-free and Cu-containing Ti-based amorphous alloys were indeed MGs with the glass transition nature. From the XRD pattern, both the Cu-free and Cu-containing Ti-based MGs appear to own amorphous structures due to the obvious diffuse hump. Only the Cu-free Ti-based MG with lower GFA compared to Cu-containing Ti-based MGs was investigated by TEM to demonstrate the homogeneously amorphous structure. Multiple bright field TEM images and selective area electron diffractions (SAED) of the $Ti_{45}Zr_{40}Zi_{15}$ ribbon were taken. The TEM results confirm the absence of any apparent nanocrystalline phase in the as-melt-spun amorphous matrix, as shown in Fig. 2.

3.2. Electrochemical response

The open circuit potential (OCP) increase with Cu content after 10,000 s immersion in the Hank's solution, $Ti_{45}Zr_{40}Si_{15}$ exhibit a lower OCP value of −0.405 V, followed by the −0.334 V for $Ti_{40}Zr_{40}Si_{15}$–Cu_5 and the −0.228 V for $Ti_{45}Zr_{20}$–Cu_{35}. The possible reason is that the standard half-cell potential of Cu is higher than Ti, Zr and Si, or Cu itself is a nobler element. Additionally, Lu et al. [35] also showed that the corrosion potential increased with increasing Cu-content in Zr–Cu MG system, which is similar to the present study. More important corrosion

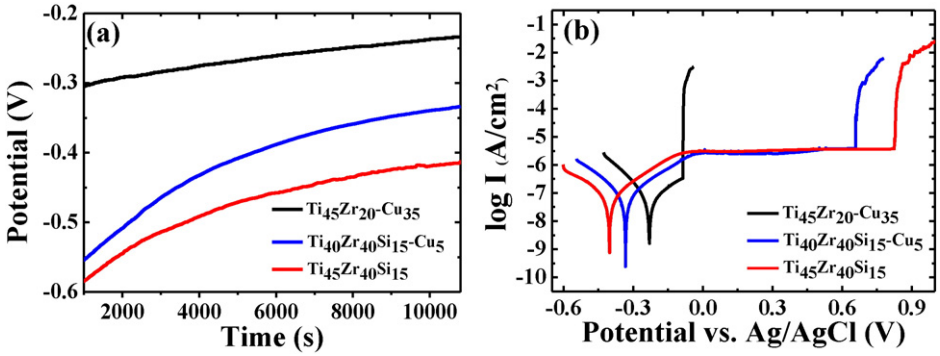

Fig. 3. (a) Open circuit potentials (OCP) and (b) potential polarization Tafel curves of the $Ti_{45}Zr_{40}Si_{15}$, $Ti_{40}Zr_{40}Si_{15}$–Cu_5 and $Ti_{45}Zr_{20}$–Cu_{35} MGs in the Hank's solution.

Table 1
Corrosion properties of the $Ti_{45}Zr_{40}Si_{15}$, $Ti_{40}Zr_{40}Si_{15}$–Cu_5 and $Ti_{45}Zr_{20}$–Cu_{35}MGs in Hank's solution. All specimens are tested three times to ensure reproducibility. The low I_{pass} reading for $Ti_{45}Zr_{20}$–Cu_{35} (about 0.4 μA/cm^2) is meaningless since the newly formed oxide layer is immediately subject to severe pitting. Each experiment was repeated for at least 3 times.

	E_{corr} (V)	E_{pit} (V)	$\Delta E = E_{pit} - E_{corr}$(V)	I_{corr} (10^{-6} A/cm^2)	I_{pass} (10^{-6} A/cm^2)
$Ti_{45}Zr_{40}Si_{15}$	−0.406 ± 0.012	0.834 ± 0.108	1.240 ± 0.120	0.078 ± 0.003	3.018 ± 0.092
$Ti_{40}Zr_{40}Si_{15}$–Cu_5	−0.325 ± 0.009	0.737 ± 0.098	1.062 ± 0.095	0.069 ± 0.005	2.963 ± 0.266
$Ti_{45}Zr_{20}$–Cu_{35}	−0.233 ± 0.004	−0.049 ± 0.009	0.184 ± 0.053	0.062 ± 0.005	–

parameters, such as corrosion potential (E_{corr}), and current density (I_{corr}), can be determined from the potentiodynamic polarizaion measurements, as shown in Fig. 3(b). E_{corr} data on $Ti_{40}Zr_{40}Si_{15}$, $Ti_{40}Zr_{40}Si_{15}$–Cu_5 and $Ti_{45}Zr_{20}$–Cu_{35} are −0.406, −0.325, and −0.233 V (Table 1), respectively, revealing the same tendency as the above OCP results. It indicates that Cu enhances the cathodic reaction and decreases the anodic reaction, leading to an increase in corrosion potential.

The SBF contains chloride ions and has been claimed to cause serious pitting reaction on the surface of amorphous alloys [36,37]. The pitting potential (E_{pit}) is a critical parameter to evaluate whether the pitting reaction would take place under a corrosive media at a critical voltage. Upon occurring pitting reaction, a sudden rising signal can be seen in the polarization curve, as shown in Fig. 3(b). The E_{pit} data are determined to be 0.834 V for $Ti_{45}Zr_{40}Si_{15}$, 0.737 V for $Ti_{40}Zr_{40}Si_{15}$–Cu_5 and −0.049 V for $Ti_{45}Zr_{20}$–Cu_{35}, also complied in Table 1. The E_{pit} of the Cu-rich $Ti_{45}Zr_{20}$–Cu_{35} is much lower than that of $Ti_{45}Zr_{40}Si_{15}$ and is even negative. With the Cu content increasing from 0 to 30 at.%, E_{pit} decreases evidently from +0.834 to −0.049 V, a decrement of 0.883 V, which is appreciable. From Huang et al. [38], defects will be formed during casting and polishing on the surface of MGs for pitting initiation. Because that the obvious difference of standard electrode potential between pure Cu (+0.52 V) and pure Ti (−0.68 V) and Zr (− 1.53 V), the nobler Cu would lead to selective dissolution against less noble Ti, Zr and Si in a Ti-based alloy system at surface defects where the Cl^- ions absorbed. In comparison, the difference of standard electrode potential between Ti, Zr and Si is not as large as the Ti, Zr, Si and Cu, revealing higher value of $E_{pit.}$ It is believed that the selective dissolution caused from diversity of electrochemical activity between different elements has resulted in the higher tendency of pitting corrosion in the Cu-containing Ti-based MGs. According to the study of Hong et al. [39], when Cu was associated with Fe, the galvanic corrosion took place. And Cu would re-deposit after dissolving. Additionally, Hong et al. [39] reported that the dissolve happened along a continuous path with less noble atoms. And also, Qin et al. [27] determined the compositions on pitting area of the Ti–Zr–Cu–Pd BMGs after polarization scanning, showing that the active element like Ti and Zr ions would dissolve into the Hank's solution preferentially leaving nobler Cu and Pd white product in the pitting region. Furthermore, Kawashima et al. [40] revealed that the pitting potential of $Zr_{70}Cu_6Al_8Ni_{16}$ is six times higher than that of $Zr_{50}Cu_{40}Al_{10}$. Moreover, comparing to the early pitting Ti–Zr–Cu–Pd MG system [27], the Cu-free Ti-based MGs fabricated by Calin et al. [8] showed no obvious pitting reaction. Other investigators and our present findings demonstrate that noble Cu in Ti-based MG matrix indeed increase the opportunity of pitting reaction.

The passive region ($\Delta E = E_{pit} - E_{corr}$) is a region for the formation of the stable oxidative layer during anodic polarization. $Ti_{45}Zr_{40}Si_{15}$ possesses the widest region (about 1.240 V) and $Ti_{45}Zr_{20}$–Cu_{35} possesses the narrowest region (only 0.184 V), as compared in Table 1. This result suggests that, with increasing Cu content in the Ti-based MGs, the protective passive oxide layers would become more prone to severe pitting.

The corrosion current density (I_{corr}) is another indication of corrosion reactivity, which of $Ti_{45}Zr_{40}Si_{15}$, $Ti_{40}Zr_{40}Si_{15}$–Cu_5 and $Ti_{45}Zr_{20}$–Cu_{35} is 0.078×10^{-6}, 0.069×10^{-6} and 0.062×10^{-6} A/cm^2, respectively, as listed in Table 1. Overall, the three values are all very close, located on the same scale (all in 10^{-8} A/cm^2). Ke et al. [41] reported the low difference (all in 10^{-8} A/cm^2) of corrosion current density between Ti–Zr–Si thin film MGs with different Ti contents. Moreover, Calin et al. [8] and Wang et al. [37] also show the similar tendency from the Ti–Zr–Si and Ti–Zr–Si–Nb MG ribbons and Zr-based BMGs. In

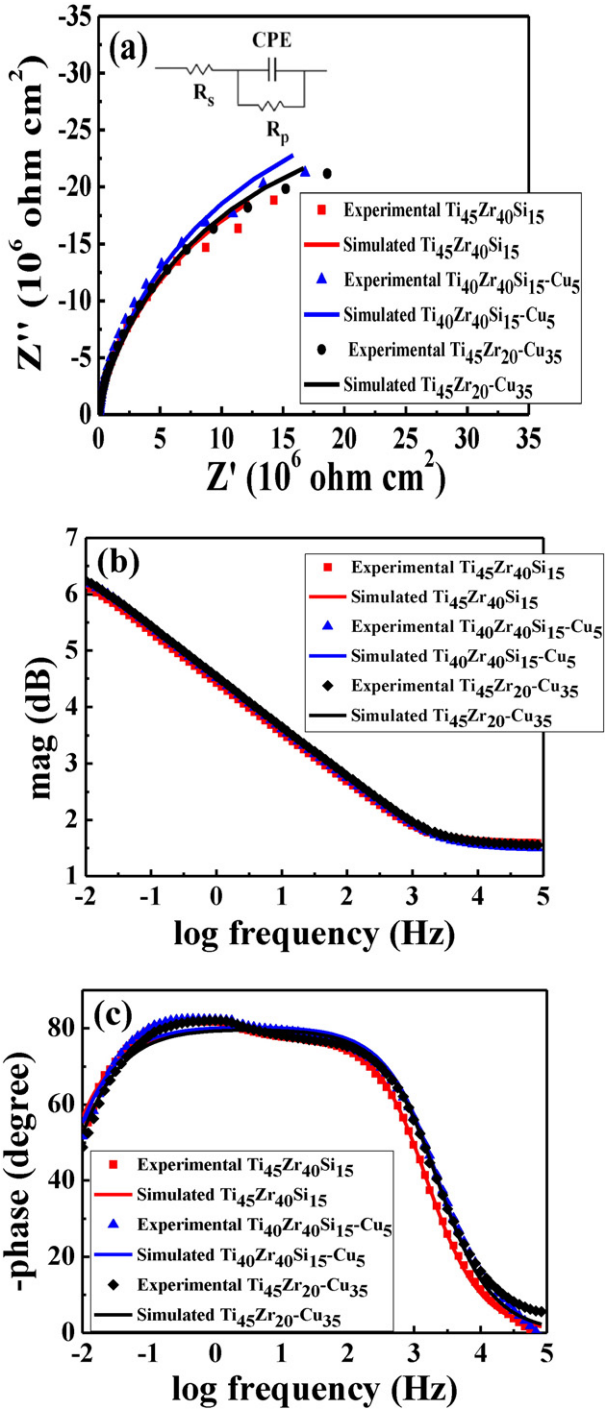

Fig. 4. The EIS spectra of the $Ti_{45}Zr_{40}Si_{15}$, $Ti_{40}Zr_{40}Si_{15}$–Cu_5 and $Ti_{45}Zr_{20}$–Cu_{35} MGs in the Hank's solution: (a) Nyquist plot, (b) Bode plot, and (c) phase angle.

Table 2
The fitting result of EIS at open circuit potential of the $Ti_{45}Zr_{40}Si_{15}$, $Ti_{40}Zr_{40}Si_{15}$–Cu_5 and $Ti_{45}Zr_{20}$–Cu_{35} MGs. Each experiment was repeated for at least 3 times.

	R_p (10^6 Ω cm^2)	Rs (10^6 Ω cm$^{2)}$	CPE-T (10^{-5}F cm^{-2})	CPE-P (F cm^{-2})	χ^2
$Ti_{45}Zr_{40}Si_{15}$	5.17 ± 0.56	6.479 ± 1.2072	4.411 ± 0.5251	5.582 ± 0.0160	0.22×10^{-2}
$Ti_{40}Zr_{40}Si_{15}$–Cu_5	5.59 ± 1.03	5.818 ± 0.7761	3.838 ± 0.36822	5.618 ± 0.0303	0.36×10^{-2}
$Ti_{45}Zr_{20}$–Cu_{35}	5.45 ± 0.44	6.572 ± 0.8134	3.426 ± 0.0167	5.523 ± 0.0373	0.46×10^{-2}

comparison, our previous work [36] on $Zr_{53}Cu_{30}Ni_9Al_8$ BMGs with different fractions of nanocrystalline phases (0% to 63%) reveals that the obvious changing in corrosion current density (10^{-5} to 10^{-7} A/cm^2) due to the formation of nanocrystals. Above results show that the structural changes in Ti-based and Zr-based MG systems seems the major issues for their current density differences. The resembling corrosion activity reveals that all of the three Ti-based MGs with or without Cu own similar homogeneously amorphous structure.

The last important parameter shown in the potentiodynamic polarization curves is the I_{pass} for evaluating whether the protective and denser passive layers were formed on the surface of the materials. The I_{pass} readings of $Ti_{45}Zr_{40}Si_{15}$ and $Ti_{40}Zr_{40}Si_{15}$–Cu_5 are similar, both around 3×10^{-6} A/cm^2, meaning that both of them can generate protective and dense passive layers on surface in the Hank's solution. Nonetheless, the pitting reaction (as presented below) of $Ti_{45}Zr_{20}$–Cu_{35} takes place too early to determine I_{pass}. The rather low I_{pass} reading (about

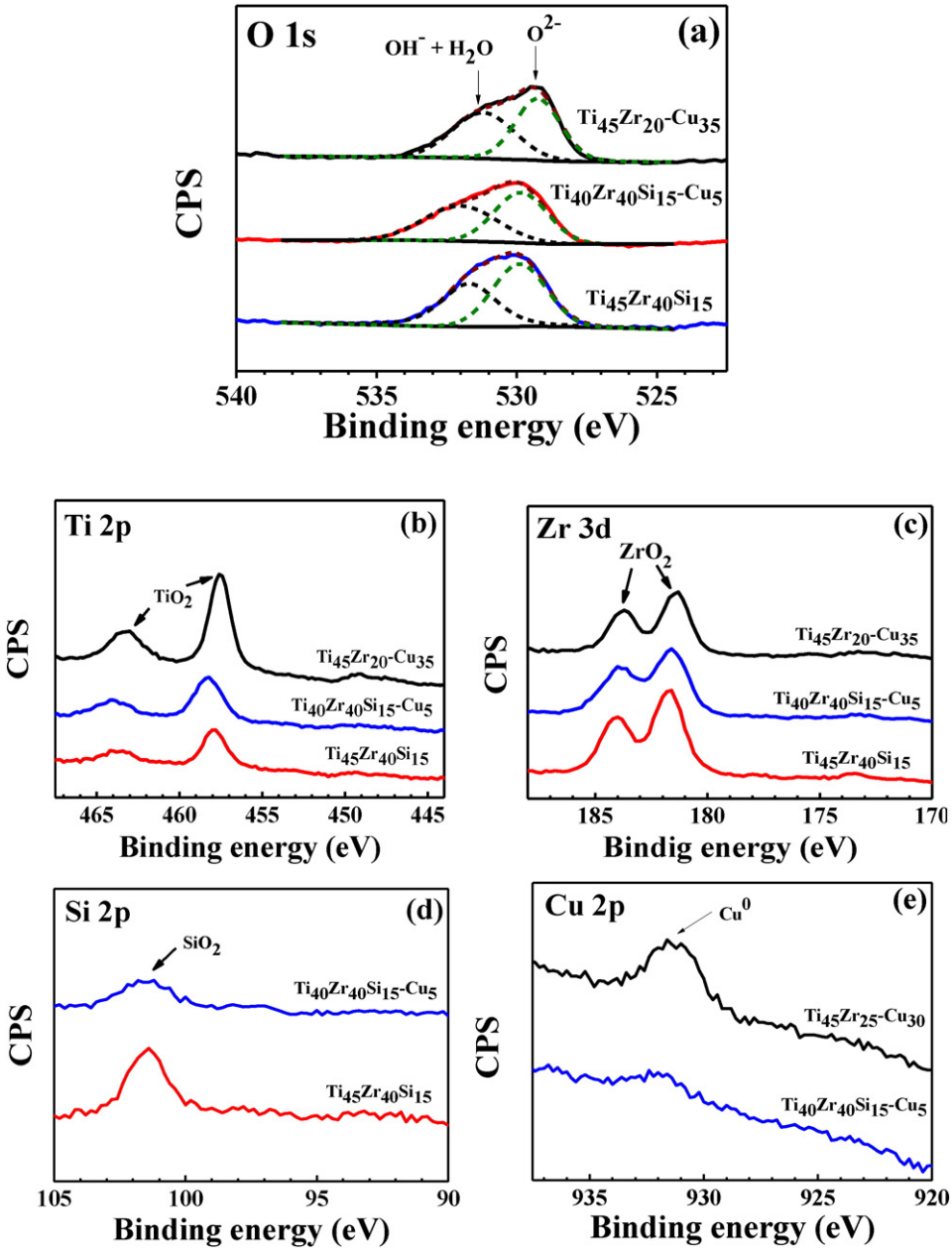

Fig. 5. XPS spectrums for the surface analysis of $Ti_{45}Zr_{40}Si_{15}$, $Ti_{40}Zr_{40}Si_{15}$–Cu_5 and $Ti_{45}Zr_{20}$–Cu_{35} after 7-day immersion in the Hank's solution: (a) O 1s, (b) Ti 2p, (c) Zr 3d, (d) Si 2p, and (e) Cu 2p peak.

0.3×10^{-6} A/cm^2) of$Ti_{45}Zr_{20}$–Cu_{35} is not meaningful, due to the fact that the passive layer once formed is immediately subjected to a serious pitting reaction. In other words, no strong passive layer was formed before pitting. The Ti-based amorphous alloys with a high content of Cu would detrimentally lead to early pitting, which is a serious drawback for such Ti-based MGs to be applied for biomedical purposes. Our previous study also shows that the Cu content should be avoided to exceed 17.5 at.% [25]. In this research, we suggest that the Cu content should keep as low as possible, better none or less than 5 at.% to reduce of pitting reactions during long-term exposure in human body.

Electrochemical impedance is a powerful method to measure resistance of electrode and electrode-solution interface and to predict the structure of passive layer of electrode [37–38,42]. By utilizing the Nyquist and Bode plots, the electrolyte resistance (R_s) and polarization resistance (R_p) of electrochemical impedance spectra (EIS) can be determined, as shown in Fig. 4. The curves of the Nyquist plot were fit by the equivalent circuit model, $R_s \cdot (CPE\text{-}R_p)$. The impedance constant phase element (CPE) is defined as $Z_{CPE} = 1/[Q(J\Omega)^n]$, where Ω is angular frequency, Q is a pre-factor of CPE, and n is its exponent with the range $0 \le n \le 1$. The quality of fitting results was judged by Chi-square (χ^2) as shown in Table 2 and the error is smaller than 5% in all case indicating the fitted data were similar to experimental results. With increasing diameter of the semi-circle in the Nyquist plot, the polarization corrosion resistance is getting higher [37]. The tendency of R_p is similar to I_{corr}, 5.17, 5.59 and 5.45 Ω for $Ti_{45}Zr_{40}Si_{15}$, $Ti_{40}Zr_{40}Si_{15}$–Cu_5 and $Ti_{45}Zr_{20}$–Cu_{35}, respectively, also compared in Table 2, indicating the similar level of electron transfer abilities. Moreover, the circuit models with one time constant show the formation of continuous one layer structure for the passive film of Cu-free and Cu-containing Ti-based MGs after 3 h immersion in the SBF. Table 1 also lists the data on Ti-based MGs with different Cu contents. It can be seen that the Cu-free $Ti_{45}Zr_{40}Si_{15}$ and low Cu-containing $Ti_{40}Zr_{40}Si_{15}$–Cu_5, in comparison with Cu-rich $Ti_{45}Zr_{20}$–Cu_{35}, exhibit slightly lower E_{corr}, similar I_{corr} and R_p, and obviously higher E_{pit}. Although the E_{corr} of Cu-free and low Cu-containing Ti-based MGs are lower than Cu-rich Ti-based MG, the Cu-free one possesses highest E_{pit} reading which confirms the more promised corrosion stability and resistance in a chloride-rich corrosive media. Besides, note that both of the I_{corr} and R_p readings are similar for the Cu-free and Cu-containing Ti-based MGs, indicating that the compositional changes of Cu will not affect the corrosion activity significantly. Only the onset of pitting will be affected due to the selective dissolution of less noble elements by noble Cu. Qin et al. [26] showed that crystalline cp Ti would own an apparently higher I_{corr} than Ti–Zr–Cu–Pd MGs, and our previous study also revealed the higher corrosion activity under Hank's solution for partially nanocrystallized Zr–Cu–Ni–Al and $Ti_{42}Zr_{40}Si_{15}Ta_3$ MGs [36,43] compared to their amorphous counterparts, suggesting that the structural defects (such as dislocations or grain boundaries) in crystalline materials are the reactive sites for electrochemical reactions. Fully amorphous MGs do not possess such defects, reducing the electrochemical responses. Therefore, the atomic structural difference, not necessarily the composition difference (Cu amount), appears to be the major factor for the I_{corr} and R_p values of MG systems.

3.3. Surface characterization and pit morphology

From the electrochemical kinetic information ΔE ($= E_{pit} - E_{corr}$) of the Cu-free and Cu-containing Ti-based MG ribbons as presented in Fig. 3(b), the passive oxide layer can be formed on the specimen surface under corrosive media. And also, the E_{pit} and E_{corr} readings reveal that the Cu-free specimens own the higher pitting resistance. To assess how the pitting resistance varies with various Cu contents, the SEM/EDS and XPS analyses were conducted.

The wide-scan and narrow-scan XPS spectra reveal the Ti, Zr, Si, Cu, O and C peaks, and the C-1s peak is originated from contaminant hydrocarbon of surface [44]. One representative narrow-scan example is shown in Fig. 5, taken from the $Ti_{40}Zr_{40}Si_{15}$–Cu_5 ribbon after long-term immersion. The apparent oxygen spectrum presented in Fig. 5(a) reveals that the board peak is composed by the dual OM and OH peaks at 529.8 and 531.7 eV, where OM is for the oxygen–metal bonding and OH is for the oxygen–hydrogen. Because of the stronger peak signal from the OM oxygen than that from the OH oxygen, the major products on the passive surfaces should be predominantly metal oxides for three Ti-based Cu-containing and Cu-free MGs. Also, the two separated peaks in Fig. 5(b) at about 464.8 and 458.8 eV correspond to the Ti^{4+} state from TiO_2, the doublet peaks in Fig. 5(c) at 184.6 and 182.2 eV are for the Zr^{4+} state from ZrO_2, the single peak in Fig. 5(d) at 101.8 eV is assigned to the Si^{4+} state from SiO_2. This indicates that the compound oxide layers made of TiO_2, ZrO_2 and SiO_2 were formed. In comparison, the single peak at 932.4 eV is Cu^0 state, as shown in Fig. 5(e), which means that Cu remains the metallic state

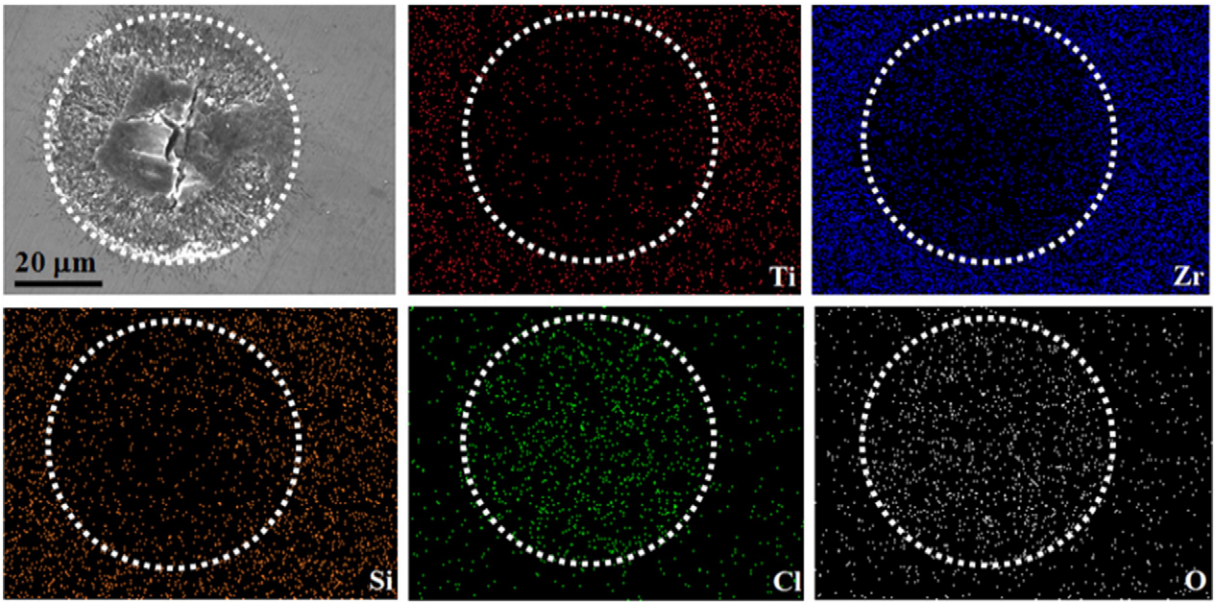

Fig. 6. Representative SEM/EDS mappings near the pitted region in the Cu-free Ti-based MGs immersed in the Hank's solution. SEM secondary electronic image showing a pitted region of $Ti_{45}Zr_{40}Si_{15}$ on the middle, and following the EDS mappings for Ti, Zr, Si, Cl, and O. Note that Ti, Zr, and Si were depleted and Cl and O were enriched in the pitted region. The white dash circles are the boundaries between pitting area and normal area on the surface of the specimens.

and un-oxidized. Wang et al. [37] also showed the similar results of un-oxidized Cu in the MG alloy system. Moreover, the XPS works on Zr-based MGs immersed in 0.5 M NaCl of Kawashima et al. [40], the peak at higher energy around 952 eV originated from Cu^0($Cu\ 2p_{3/2}$) is rather weak compared to peak around 932 eV originated from Cu^+ ($Cu\ 2p_{1/2}$). Hence, we suggest that the Cu is hard to be oxidized during 7 days immersion under Hank's solution. After immersing in SBF for 7 days, elements of Ti, Zr and Si in the Cu-free and Cu-containing alloy systems are all oxidized except Cu, indicating that Cu is indeed nobler than the others. Consequently, E_{corr} would increase and E_{pit} would decrease

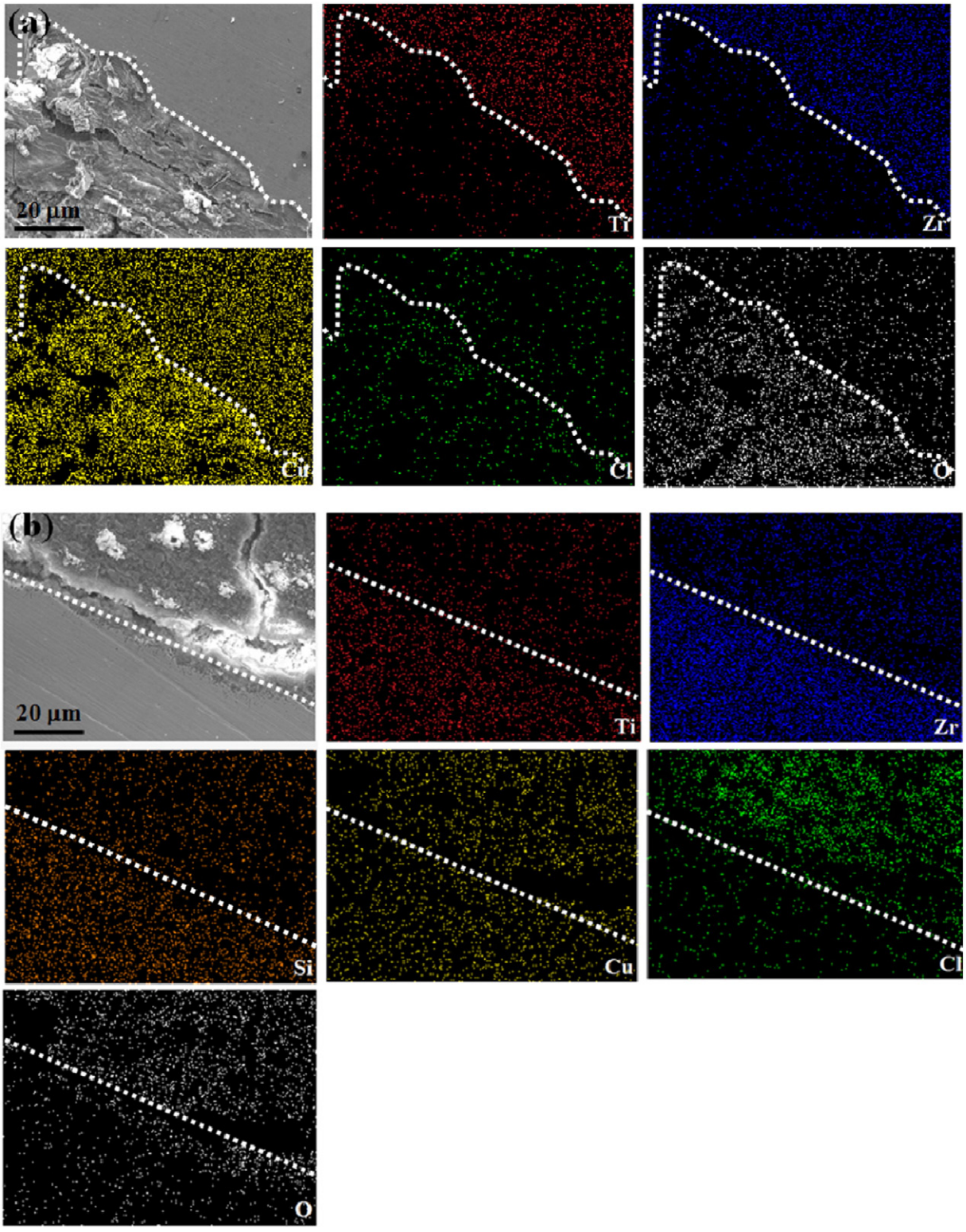

Fig. 7. Representative SEM/EDS mappings near the pitted region in the Cu-contained Ti-based MGs immersed in the Hank's solution. (a) SEM secondary electronic image showing a pitted region of $Ti_{45}Zr_{20}$–Cu_{35}on the lower left side, and the EDS mappings for Ti, Zr, Cu, Cl, and O. (b) SEM secondary electronic image showing a pitted region of $Ti_{40}Zr_{40}Si_{15}$–Cu_5, and the EDS mappings for Ti, Zr, Si, Cu, Cl, and O. Note that Ti, Zr, and Si were depleted and Cu, Cl and O were enriched in the pitted region. The white dash lines are the boundaries between pitting area and normal area on the surface of the specimens.

Table 3
Measured concentration variation (ppm) for the target ions in the mediums after the potential state tests at an applied voltage of 80 mV.

	Ti (ppm)	Zr (ppm)	Cu (ppm)	Si (ppm)
$Ti_{45}Zr_{40}Si_{15}$	0.003	0.003	–	0.410
$Ti_{40}Zr_{40}Si_{15}$–Cu_5	0.006	0.026	0.015	1.066
$Ti_{45}Zr_{20}$–Cu_{35}	23.526	15.297	0.500	–

with increasing Cu content in an alloy system, due to the Cu-induced larger activity energy of passivation and serious selective dissolution. In this study, the surface compositions of the three Ti-based alloys are composed of TiO_2, ZrO_2 and SiO_2 for $Ti_{45}Zr_{40}Si_{15}$, TiO_2, ZrO_2, SiO_2 and Cu for $Ti_{40}Zr_{40}Si_{15}$–Cu_5, and TiO_2, ZrO_2 and Cu for $Ti_{45}Zr_{20}$–Cu_{35}, respectively. With abundant un-oxidized Cu in $Ti_{45}Zr_{20}$–Cu_{35}, preferential pitting would occur for this amorphous ribbon.

The representative examples of the SEM/EDS mappings are shown in Figs. 6 and 7(a)–(b), and the boundaries between the pitting reaction regions were labeled by dash lines for better recognition. To determine possible products and the distribution of Ti, Zr, Si, Cu, O, and Cl after pitting reaction, we use majorly the region without pitting as a standard to compare with the region with pitting. For the Cu-free Ti-based MG, $Ti_{45}Zr_{40}Si_{15}$, Ti, Zr and Si would be dissolved at highest E_{pit} (above E_{pit} ~ 0.834 V), making Ti, Zr and Si be preferentially corroded away by Cl, leaving the lower Ti, Zr and Si and enriched Cl and O distributions in the pitted area, as shown in Fig. 6. For the Cu-containing $Ti_{45}Zr_{20}$–Cu_{35} and $Ti_{40}Zr_{40}Si_{15}$–Cu_5, selective dissolution will be induced at lower E_{pit} (at applied voltage ~ 0.737 V and −0.049 V for $Ti_{40}Zr_{40}Si_{15}$–Cu_5 and $Ti_{45}Zr_{20}$–Cu_{35}) than Cu-free $Ti_{45}Zr_{40}Si_{15}$, between both Ti and Cu, and Zr and Cu, as well as Si and Cu, resulting in the preferential lower Ti, Zr and Si and enriched Cu, and Cl and O contents in the pitted regions as exampled in Figs. 7(a)–(b). In comparison, the pitting reaction for $Ti_{45}Zr_{20}$–Cu_{35} occurs at lowest E_{pit} compared to $Ti_{45}Zr_{40}Si_{15}$ and $Ti_{40}Zr_{40}Si_{15}$–Cu_5, selectively dissolving the Ti and Zr away by Cl, revealing lower contents of Ti and Zr and higher contents of Cu, Cl and O. Meanwhile, noble Cu in Ti-based amorphous matrix will increase the opportunity of pitting reaction. Furthermore, Cl and O will be enriched in the pitted area upon corrosion in the Cl-containing SBF solution due to the serious pitting and oxidized reaction. Since Ti ions have been reported to form Ti–OH groups [45], it is possible that some other products such as calcium-phosphate might have formed in the pitted regions.

Our previous results [25,36] have shown that the reactive elements will be dissolved more readily due to the high Cu content in the Zr-based MGs, which is consistent with the reports by Huang et al. [38] and Kawashima et al. [40]. According to present results, the preferential dissolution by Cu also occurs on Ti-based MGs. From the above discussion and modeling, it is clear that the presence of nobler Cu will impose two opposite effects. The positive effect comes from the nobler nature of Cu, which would start the polarization reaction at a higher voltage level, for example, from E_{corr} ~ −0.4 V for the Cu-free $Ti_{45}Zr_{40}Si_{15}$ to E_{corr} ~ −0.2 V for the Cu-containing $Ti_{45}Zr_{20}$–Cu_{35}. The negative effect is the induction of severe Cu-induced selective dissolution under SBF with lower applied voltage levels compared to Cu-free Ti-based MGs, resulting in continuous pitting and the depletion of Ti, Zr or Si in the alloy. The minor difference of E_{corr} for is in fact not a major issue for evaluating the corrosion resistance. But the negative effect on local pitting and ion release would cause a major drawback due to the obvious disparity of E_{pit}. It is suggested that the Cu content should be kept as low as one can or better to be none for improving the anti-pitting ability of Ti-based MG systems.

Additionally, in order to validate the possible ion released from Ti-based MGs, ICP-MS was conducted to measure the concentration variation (ppm) for target ions in the solution prior to and after potential state test under membrane potential (80 mV), as shown in Table 3. The toxic Cu concentration of $Ti_{45}Zr_{20}$–Cu_{35} was about 30 times higher than low Cu-containing $Ti_{40}Zr_{40}Si_{15}$–Cu_5. Results show that the Cu-rich Ti-based MG system will release harmful Cu ions under SBF via serious pitting corrosion. According to Lin et al. [25] result, MGs with higher Cu content owns lower cell viability, indicating Cu do harm to D1 cell decreasing the biocompatibility. Besides, the Cu free MGs not only process good electrochemical stability under cell membrane potential but have no obvious impact on viability of D1 cell as well, suggesting the promised biocompatibility of Cu free MGs. Therefore, reducing Cu content in Ti-based MG system can greatly improve their biocompatibility for biomedical implantation.

4. Conclusion

Although the Cu-free Ti-based MGs are difficult to be prepared into a bulk form, the effect of the different Cu content on corrosion resistance in the Ti-based MG ribbon under SBF can still provide useful information for the compositional design of Ti-based MGs. It is assured that the Cu addition can improve GFA, it would nevertheless reduce the corrosion resistance in SBF. The systematic characterization of the corrosion response of the Cu-free $Ti_{45}Zr_{40}Si_{15}$ and Cu-containing $Ti_{40}Zr_{40}Si_{15}$–Cu_5 and $Ti_{45}Zr_{20}$–Cu_{35}MGs in the Hank's solution is conducted. Based on the open circuit potential (OCP), potentiodynamic polarization measurements, electrochemical impedance measurements, XPS analysis, SEM/EDS mapping, as well as ICP-MS, the following conclusions can be drawn.

(1) The positive effect of the addition of Cu in the Ti-based MGs comes from the nobler nature of Cu, which would shift the beginning of polarization reaction to a higher voltage level, for example, from E_{corr} ~ −0.4 V for the Cu-free $Ti_{45}Zr_{40}Si_{15}$ to E_{corr} ~ −0.2 V for the Cu-containing $Ti_{45}Zr_{20}$–Cu_{35}.
(2) The negative effect is the induction of severe Cu-induced selective dissolution under the higher applied voltage levels, resulting in continuous pitting and the depletion of Ti, Zr or Si in the alloy.
(3) It is clear that the presence of nobler Cu will impose the above two opposite effects. The minor positive shift of E_{corr} comes from nobler nature of Cu is in fact not a major issue. But the negative effect on local pitting and ion release would cause a major drawback. The result of ICP-MS shows that the bio-toxic Cu ions released from Cu-rich Ti-based MGs. It is suggested that the Cu content should be kept as low as one can, none or less than about 5 at.%, to ensure the absence of pitting during long-term exposure in human body.
(4) A minor addition of about 5 at.% Cu might be the compromise for the contradictive consideration of glass forming ability and biocompatibility. The 5 at.% Cu can appreciably upgrade the GFA but not harm much the biocompatibility.

Acknowledgment

The authors gratefully acknowledge the support from the Ministry of Science and Technology of Taiwan, ROC, under grants NSC101-2112-M-110-004 and NSC 98-2221-E-110-035-MY3. The helps by J. B. Li and H. C. Lin of National Central University of Taiwan on the melt spinning and Y. S. Huang of National Sun. Yat-Sen University on ICP-MS work are gratefully acknowledged.

References

[1] U.K. Mudali, T.M. Sridhar, B. Raj, Sadhana Acad. Proc. Eng. Sci. 28 (2003) 601–637.
[2] S.R. Paital, N.B. Dahotre, Mater. Sci. Eng. R 66 (2009) 1–70.
[3] I. Gotman, J. Endourol. 11 (1997) 383–389.
[4] Y. Tsutsumi, S. Bartakova, P. Prachar, Suyalatu, S. Migita, H. Doi, N. Nomura, T. Hanawa, J. Electrochem. Soc. 159 (2012) C435–C440.
[5] M. Long, H.J. Rack, Biomaterials 19 (1998) 1621–1639.
[6] S. Karimi, A.M. Alfantazi, J. Electrochem. Soc. 160 (2013) C206–C214.
[7] K. Doi, S. Miyabe, S. Fujimoto, J. Electrochem. Soc. 160 (2013) C576–C580.

[8] M. Calin, A. Gebert, A.C. Ghinea, P.F. Gostin, S. Abdi, C. Mickel, J. Eckert, Mater. Sci. Eng. C 33 (2013) 875–883.
[9] T. Hanawa, Mater. Sci. Eng. C 24 (2004) 745–752.
[10] Y. Okazaki, E. Gotoh, Biomaterials 26 (2005) 11–21.
[11] H.J. Agins, N.W. Alcock, M. Bansal, E.A. Salvati, P.D. Wilson, P.M. Pellicci, P.G. Bullough, J. Bone Joint Surg. 70A (1988) 347–356.
[12] M.A. Khan, R.L. Williams, D.F. Williams, Biomaterials 17 (1996) 2117–2126.
[13] T. Kodama, Kokubyo Gakkai zasshi, J. Stomatol. Soc. Jpn. 56 (1989) 263–288.
[14] D.R.C. McLachlan, C. Bergeron, J.E. Smith, D. Boomer, S.L. Rifat, Neurology 48 (1997) 1141–1142.
[15] K.L. Wapner, Clin. Orthop. Relat. Res. 271 (1991) 12–20.
[16] A. Inoue, T. Zhang, T. Masumoto, Mater. Trans. JIM 36 (1995) 391–398.
[17] A. Inoue, Mater. Trans. JIM 36 (1995) 866–875.
[18] D.P. Wang, S.L. Wang, J.Q. Wang, Corros. Sci. 59 (2012) 88–95.
[19] C. Li, D. Chen, W. Chen, L. Wang, D. Luo, Corros. Sci. 84 (2014) 96–102.
[20] Y.B. Wang, H.F. Li, Y.F. Zheng, M. Li, Mater. Sci. Eng. C 32 (2012) 599–606.
[21] H.C. Lin, P.H. Tsai, J.H. Ke, J.B. Li, J.S.C. Jang, C.H. Huang, J.C. Huang, Intermetallics 55 (2014) 22–27.
[22] H.H. Huang, Y.S. Sun, Y.S. Wu, C.P. Liu, P.K. Liaw, K. Wu, Intermetallics 30 (2012) 139–143.
[23] M.L. Morrison, R.A. Buchanan, R.V. Leon, C.T. Liu, B.A. Green, P.K. Liaw, J.A. Horton, J. Biomed. Mater. Res. A 74A (2005) 430–438.
[24] J.R. Scully, A. Gebert, J.H. Payer, J. Mater. Res. 22 (2007) 302–313.
[25] C.H. Lin, C.H. Huang, J.F. Chuang, J.C. Huang, J.S.C. Jang, C.H. Chen, Mater. Sci. Eng. C 33 (2013) 4520–4526.
[26] J. Fornell, N. Van Steenberge, A. Varea, E. Rossinyol, E. Pellicer, S. Surinach, M.D. Baro, J. Sort, J. Mech. Behav. Biomed. Mater. 4 (2011) 1709–1717.
[27] F.X. Qin, M. Yoshimura, X.M. Wang, S.L. Zhu, A. Kawashima, K. Asami, A. Inoue, Mater. Trans. JIM 48 (2007) 1855–1858.
[28] T. Zhang, A. Inoue, T. Masumoto, Mater. Sci. Eng. A 182 (1994) 1423–1426.
[29] A. Inoue, N. Nishiyama, K. Amiya, T. Zhang, T. Masumoto, Mater. Lett. 19 (1994) 131–135.
[30] K. Amiya, N. Nishiyama, A. Inoue, T. Masumoto, Mater. Sci. Eng. A 179 (1994) 692–696.
[31] Y.C. Kim, W.T. Kim, D.H. Kim, Mater. Sci. Eng. A 375 (2004) 127–135.
[32] W.M. Elshahawy, I. Watanabe, P. Kramer, Dent. Mater. 25 (2009) 1551–1555.
[33] J.J. Oak, A. Inoue, Mater. Sci. Eng. A 449 (2007) 220–224.
[34] J.C. Hornez, A. Lefèvre, D. Joly, H.F. Hildebrand, Biomol. Eng. 19 (2002) 103–117.
[35] H.B. Lu, L.C. Zhang, A. Gebert, L. Schultz, J. Alloys Compd. 462 (2008) 60–67.
[36] C.H. Huang, J.C. Huang, J.B. Li, J.S.C. Jang, Mater. Sci. Eng. C 33 (2013) 4183–4187.
[37] Y.B. Wang, Y.F. Zheng, S.C. Wei, M. Li, J. Biomed. Mater. Res. Part B 96B (2011) 34–46.
[38] L. Huang, D. Qiao, B.A. Green, P.K. Liaw, J. Wang, S. Pang, T. Zhang, Intermetallics 17 (2009) 195–199.
[39] J.H. Hong, S.H. Lee, J.G. Kim, J.B. Yoon, Corros. Sci. 54 (2012) 174–182.
[40] A. Kawashima, K. Ohmura, Y. Yokoyama, A. Inoue, Corros. Sci. 53 (2011) 2778–2784.
[41] J.L. Ke, C.H. Huang, Y.H. Chen, W.Y. Tsai, T.Y. Wei, J.C. Huang, Appl. Surf. Sci. 322 (2014) 41–46.
[42] R. Menini, M.J. Dion, S.K.V. So, M. Gauthier, L.P. Lefebvre, J. Electrochem. Soc. 153 (2006) B13–B21.
[43] C.H. Huang, J.J. Lai, T.Y. Wei, Y.H. Chen, X. Wang, S.Y. Kuan, J.C. Huang, Mater. Sci. Eng. C 52 (2015) 144–150.
[44] F.X. Qin, X.M. Wang, A. Kawashima, S.L. Zhu, H. Kimura, A. Inoue, Mater. Trans. JIM 47 (2006) 1934–1937.
[45] P. Li, P. Ducheyne, J. Biomed. Mater. Res. A 41 (1998) 341–348.